Miner Petrol (2017) 111:363–372
DOI 10.1007/s00710-016-0484-9

ORIGINAL PAPER

Zincobotryogen, $ZnFe^{3+}(SO_4)_2(OH)\cdot 7H_2O$: validation as a mineral species and new data

Zhuming Yang[1] · Gerald Giester[2] · Qian Mao[1] · Yuguang Ma[1] · Di Zhang[1] · He Li[1]

Received: 22 June 2016 / Accepted: 4 November 2016 / Published online: 19 November 2016

Abstract Zincobotryogen occurs in the oxidation zone of the Xitieshan lead-zinc deposit, Qinghai, China. The mineral is associated with jarosite, copiapite, zincocopiapite, and quartz. The mineral forms prismatic crystals, 0.05 to 2 mm in size. It is optically positive ($2V_{calc} = 54.1°$), with Z ∥ *b* and X ∧ *c* = 10°. The elongation is negative. The refractive indices are $n_\alpha = 1.542(5)$, $n_\beta = 1.551(5)$, $n_\gamma = 1.587(5)$. The pleochroism scheme is X = colorless, Y = light yellow, Z = yellow. Microprobe analysis gave (in wt%): $SO_3 = 38.04$, $Al_2O_3 = 0.04$, $Fe_2O_3 = 18.46$, ZnO = 13.75, MgO = 1.52, MnO = 1.23, $H_2O = 31.06$ (by calculation), Total = 104.10. The simplified formula is $(Zn,Mg)Fe^{3+}(SO_4)_2(OH)\cdot 7H_2O$. The mineral is monoclinic, $P12_1/n1$, $a = 10.504(2)$, $b = 17.801(4)$, $c = 7.1263(14)$ Å, and $\beta = 100.08(3)°$, $V = 1311.9(5)$ Å^3, Z = 4. The strongest lines in the powder X-ray diffraction pattern *d*(I)(*hkl*) are: 8.92 (100)(110), 6.32 (77)(−101), 5.56 (23)(021), 4.08 (22)(−221),3.21 (31)(231), 3.03 (34)(032), 2.77 (22)(042). The crystal structure was refined using 2816 unique reflections to $R1(F) = 0.0355$ and $wR2(F^2) = 0.0651$. The refined formula is $(Zn_{0.84}Mg_{0.16})Fe^{3+}(SO_4)_2(OH)\cdot 7H_2O$. The atomic arrangement is characterized by chains with composition $[Fe^{3+}(SO_4)_2(OH)(H_2O)]^{2-}$ and ~ 7 Å repeat distance running parallel to the *c*-axis. The chain links to a $[MO(H_2O)_5]$ octahedron (*M* = Zn, Mg) and an unshared H_2O molecule, and forms a larger chain building module with composition $[M^{2+}Fe^{3+}(SO_4)_2(OH)(H_2O)_6(H_2O)]$. The inter-chain module linkage involves only hydrogen bonding.

Keywords Zincobotryogen · New mineral · Hydrated sulfate · Crystal-structure refinement · Hydrogen bonds

Editorial handling: N. V. Chukanov

✉ Gerald Giester
gerald.giester@univie.ac.at

[1] Institute of Geology and Geophysics, Chinese Academy of Sciences, P.O. Box 9825, Beijing 100029, China

[2] Institut für Mineralogie und Kristallographie, Universität Wien, Althanstraße 14, 1090 Wien, Austria

Introduction

Botryogen, $MgFe^{3+}(SO_4)_2(OH)\cdot 7H_2O$, is a hydrated sulfate of magnesium and ferric iron. Recently, Majzlan et al. (2016) investigated samples from Nuevo Cuyo, Argentina with chemical composition $MFe^{3+}{}_{1.010}(SO_4)_2(OH)\cdot 7H_2O$ with $M = Mg_{0.773}Zn_{0.165}Mn_{0.047}$. However, botryogen from Rammelsberg mine, Germany, had been reported to have a formula as $(Zn,Mn,Mg,Fe^{2+})Fe^{3+}(SO_4)_2(OH)\cdot 7H_2O$ (Zemann 1961). The crystal structure of this mineral was determined with all non-H atoms positions using the sample from the Rammelsberg mine by Süsse (1967, 1968) in the space group $P2_1/n$ with unit cell dimensions of $a = 10.526(4)$, $b = 17.872(7)$, $c = 7.136(4)$ Å, and $\beta = 100.13(4)°$. On the basis of chemical composition the formula for this mineral was given as $(Zn_{0.47}Mn_{0.25}Mg_{0.20}Fe^{2+}{}_{0.08})_{\Sigma 1.00}Fe^{3+}(SO_4)_2(OH)\cdot 7H_2O$. Although zinc is the predominant element in the *M* site, this mineral species was labeled as botryogen, $MgFe^{3+}(SO_4)_2(OH)\cdot 7H_2O$. Furthermore, the name of botryogen-Zn is used to describe the sample from Mina Quetena, Calama, Chile (Lane et al. 2015).

Zincobotryogen, $(Zn_{0.65}Mg_{0.28}Mn_{0.11}Fe_{0.05}Na_{0.01})_{\Sigma 1.10}Fe^{3+}{}_{1.03}(SO_4)_{2.02}(OH)_{1.24}\cdot 6.68H_2O$, was firstly reported as a variety of botryogen from the Xitieshan lead-zinc deposit, Qinghai Province, China (Tu et al. 1964a,b). Mössbauer and Infrared (IR) spectra as well as investigations by thermogravimetry (TG) and differential thermal analysis

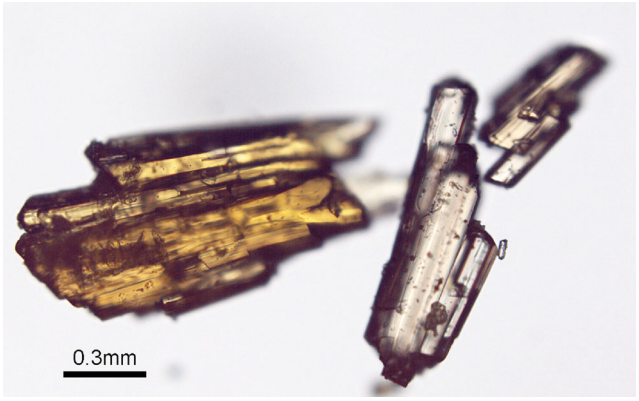

Fig. 1 Photomircograph (cross-polarized transmitted light) of several groups of zincobotryogen crystals

Table 1 Chemical composition of zincobotryogen (10 analyses)

Constituent	Mean [wt%]	Range [wt%]	SD	EPMA calibrant
SO_3	38.0	37.24–38.46	0.34	Baryte
Al_2O_3	0.04	0 –0.10	0.03	Corundum
Fe_2O_3	18.5	18.22–18.82	0.24	Hematite
ZnO	13.8	12.95–14.82	0.60	Synthetic ZnO
MgO	1.52	1.37–1.86	0.15	Diopside
MnO	1.23	1.03–1.96	0.27	Rhodonite
H_2O[a]	31.1			
Total	104.1			

[a] Calculated on the basis of $(H_2O) = 7$ *pfu* and O in (SO_4) + (OH) groups = 9 *apfu*

SD standard deviation

(DTA) for zincobotryogen were given by Yang and Fu (1988a). The crystal structure of zincobotryogen was determined, but without refinement of the (Zn, Mg) site populations and without hydrogen atoms locations (Yang and Fu 1988b). The unit cell reported was: $a = 10.52(1)$, $b = 17.85(2)$, $c = 7.133(5)$ Å, and $\beta = 100.14(6)°$ with space group $P2_1/n$. However, according to the list of mineral species compiled by the Commission on New Minerals, Nomenclature and Classification, International Mineralogical Association (CNMNC, IMA), zincobotryogen was not regarded as a valid mineral species so far.

In the present study, using the original sample of zincobotryogen from the Xitieshan lead-zinc deposit, chemical analyses were performed by an electron microprobe analyzer and the crystal structure was reinvestigated. All atoms including hydrogen atoms have been located and the hydrogen bounding system is discussed. The (Zn, Mg) site population has been refined, confirming that zincobotryogen is deserved as a mineral species. The new mineral and its name have been approved by the CNMNC, IMA (IMA No. 2015–107). The mineral is named after its chemical composition and relationship to botryogen. The type specimen of zincobotryogen has been deposited in the mineralogical collection of the Museum, Institute of Geology and Geophysics, Chinese Academy of Sciences with registration number, KDX076.

General description of zincobotryogen

Mineral occurrence

The Xietieshan lead-zinc deposit is located at the northern margin of the Qaidam Basin, Qinghai Province, China, and distributed in the Upper Ordovician Tanjianshan Group volcanic-sedimentary rocks. The Tanjianshan Group is separated by a fault from the Meso- to Neo-Proterozoic Dakendaben Group mica-quartz schists to the northeast and unconformable overlain by Devonian-Carboniferous purple conglomerates. The Tanjianshan Group is divided into three formation units from bottom upward: (1) volcanic-sedimentary rocks, (2) purple sandstone, and (3) intermediate-basic volcanic rocks. The Pb-Zn ore bodies are hosted in the marble and greenschists of the lower formation unit. The minerals in the deposit are mainly sphalerite, galena, pyrite and calcite; the minor minerals are quartz, dolomite,

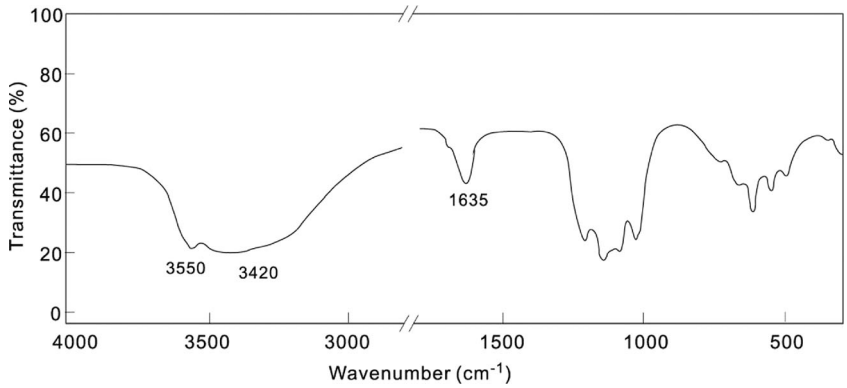

Fig. 2 Infrared-absorption spectrum of zincobotryogen

Table 2 X-ray powder diffraction data of zincobotryogen

I	d_{meas}(Å)	d_{Calc}(Å)	h	k	l
100	**8.92**	**8.92**	**1**	**1**	**0**
77	**6.32**	**6.41**	**−1**	**0**	**1**
23	**5.56**	**5.53**	**0**	**2**	**1**
45	**5.14**	**5.14**	**1**	**1**	**1**
13	4.40	4.36	−1	3	1
22	**4.08**	**4.08**	**−2**	**2**	**1**
20	3.76	3.77	0	4	1
17	3.54	3.53	0	0	2
10	3.37	3.37	2	4	0
31	**3.21**	**3.22**	**2**	**3**	**1**
34	**3.03**	**3.03**	**0**	**3**	**2**
22	**2.77**	**2.77**	**0**	**4**	**2**
4	2.57	2.57	2	2	2
11	2.48	2.48	−4	2	1
6	2.37	2.37	−4	3	1
2	2.25	2.25	3	6	0
7	2.17	2.17	−3	5	2
12	2.06	2.06	1	8	1
1	1.97	1.97	−5	3	1
2	1.90	1.90	4	1	2
8	1.79	1.79	−1	1	4
3	1.72	1.73	−3	8	2
5	1.59	1.59	−2	5	4
2	1.52	1.52	−5	8	1
6	1.45	1.45	−7	1	2
1	1.41	1.41	3	11	1
2	1.28	1.28	−1	13	2
1	1.22	1.22	3	2	5
1	1.18	1.18	6	11	0
3	1.12	1.12	−2	10	5
1	1.04	1.04	6	10	3
1	0.95	0.95	9	3	3

Parameters of the most intense powder diffraction lines are quoted bold

Table 3 Crystal data, data collection information and refinement details for zincobotryogen

Formula	$(Zn_{0.84}Mg_{0.16})Fe(SO_4)_2(OH) \cdot 7H_2O$
Formula weight	449.73
Space group	$P12_1/n1$
a (Å)	10.504(2)
b (Å)	17.801(4)
c (Å)	7.1263(14)
β (°)	100.08(3)
V (Å^3), Z	1311.9(5), 4
μ (mm^{-1})	3.052
Crystal dimensions (mm^3)	0.14 × 0.11 × 0.10
F (000), ρ_{calc}(g·cm^{-3})	912, 2.277
λ (Mo$K\alpha$)(A), T(K)	0.71073, 293(2)
θ range for collection	3.41 to 27.50°
Number of frames	1000
Scan time (s/°)	5
h,k,l ranges	−13 → 13, −23 → 23, −9 → 9
Total reflections measured	14234
Unique reflections	2995 [R(int) =3.88 %]
Reflections used	2816 with $I > 2\sigma(I)$
Refinement on	F^2
$R1(F)$, w$R2(F^2)$[I>2σ(I)]	3.55 %, 6.51 %
No. of refined parameters	232
GoF on F^2	1.197
Δρmin, Δρmax (e/Å^3)	−0.40, 0.37

RigakuFour-circle diffractometer equipped with a Saturn 724+ CCD detector, Mo tube, graphite monochrometor, φ-scans for distinct ω-angles, Δφ = 0.5°/frame, frame size: binned mode, 34 μm/2048 × 2048 pixels, detector-to sample distance: 45 mm. Unit-cell parameters were obtained by least-squares refinements of 2θ values

chlorite, pyrrhotite, chalcopyrite, marcasite and arsenopyrite (Wang et al. 2008).

In the area of the Xietieshan lead-zinc deposit the climate is very arid. The average annual precipitation is below 100 mm and the evaporation capacity is usually up to 2000 mm. The oxidation zone of the lead-zinc deposit is well developed, and the thickness varies from 4 to 20 m. The oxidation zone can be divided into three vertical subzones in the profile from top downward: (1) Limonite-hematite subzone with the thickness of 2–5 cm, (2) Jarosite subzone with the thickness of 3–20 m, consisting of jarosite, quartz, gypsum, sulfur, anglesite, copiapite, zincocopiapite, sideronatrite and fibroferrite, and (3) Gypsum-sulfur subzone with the thickness of 1–4 m, consisting of gypsum, sulfur, anglesite, quartz, melanterite, roemerite and halotrichite. Zincobotryogen occurs in the Jarosite subzone, associated with jarosite, copiapite, zincocopiapite, and quartz (Tu and Li 1963; Tu et al. 1964a, b).

The spatial distribution of sulphate minerals shows a rather definite pattern in the oxidation zone of the Pb-Zn deposit: ferric sulphates are observed in the Jarosite subzone containing copiapite, sideronatrite and fibroferrite, while ferrous sulphates have their prominent development in the Gypsum-sulfur subzone containing melanterite, roemerite and halotrichite. Zn-bearing sulphate minerals, such as zincocopiapite and zincobotryogen, mainly occur in the Jarosite subzone, Mg-bearing sulphate minerals, such as pickeringite, in the Gypsum-sulfur subzone.

Physical and optical properties

The mineral forms prismatic crystals elongated in [001] from 0.5 to 2 mm in length and 0.05 to 0.2 mm in diameter, and commonly occurs in radial or globular aggregates (Fig. 1). The crystals are transparent; their colors are light to dark

orange-red. The streak of zincobotryogen is light yellow, and its luster is vitreous. The density of crystal aggregates measured by using a micro-torsion balance is 2.20(1) g/cm^3 and the calculated crystal density (for Z = 4) is 2.266 g/cm^3. The mineral is soluble in hot water similar to botryogen.

Zincobotryogen is prismatic, with observed forms: {010}, {$\bar{1}$01}, {120}, and {110}. The a:b:c ratio calculated from the single-crystal unit cell parameters is 0.5901:1:0.4003.

Zincobotryogen is optically positive ($2V_{calc}$ = 54.1°), with Z ∥ *b* and X ∧ *c* = 10°. The elongation is negative. The refractive indices, measured in Na-light, are n_α = 1.542(5), n_β = 1.551(5), n_γ = 1.587(5). The pleochroism scheme is: X = colorless, Y = light yellow, Z = yellow. The dispersion is strong with r > v. The compatibility factor calculated from the Gladstone-Dale rule (Mandarino 1981) is superior (0.006).

Chemical composition

The quantitative chemical composition of zincobotryogen was measured with a JXA-8100 electron microprobe analyzer in wavelength-dispersive spectroscopic (WDS) mode. Accelerating voltage and specimen current were kept at 15 kV and 10 nA. The beam diameter was 5 μm. The chemical composition was determined from ten electron microprobe analyses shown in Table 1. The H_2O content was calculated from charge balance and theoretical content of water molecules. The high analytical total is attributed to partial dehydration under vacuum either during carbon coating or in the microprobe chamber. This H_2O loss results in higher concentrations for the remaining constituents than are to be expected for the fully hydrated phase.

The empirical formula, based on 16 O *apfu*, is $(Zn_{0.73}Mg_{0.16}Mn_{0.08})_{\Sigma 0.97}Fe^{3+}_{0.99}(SO_4)_{2.04}(OH)_{0.82}\cdot 7H_2O$. The simplified formula is $(Zn,Mg)Fe^{3+}(SO_4)_2(OH)\cdot 7H_2O$. The ideal one is $ZnFe^{3+}(SO_4)_2(OH)\cdot 7H_2O$, with a theoretical chemical composition (in wt%): SO_3 = 35.08, Fe_2O_3 = 17.49, ZnO = 17.83, H_2O = 29.60, Total = 100.00. The chemical composition of the same sample including the concentration of H_2O and the Fe valence state was obtained by wet chemical analysis (Tu et al. 1964b) (in wt%): SO_3 = 36.03, Al_2O_3 = 0.01, Fe_2O_3 = 18.34, FeO = 0.85, ZnO = 11.77, MgO = 2.50, MnO = 1.75, Na_2O = 0.05, H_2O = 29.35, Total = 100.65. The empirical formula, based on 16 O *apfu*, is $(Zn_{0.65}Mg_{0.28}Mn_{0.11}Fe_{0.05}Na_{0.01})_{1.10}Fe^{3+}_{1.03}(SO_4)_{2.02}(OH)_{1.24}\cdot 6.68H_2O$.

Our TG and DTA data indicate that zincobotryogen loses most of (H_2O) at 149 °C i.e., 28.2 wt% (Yang and Fu 1988a). The loss of (OH) is initiated at 475 °C and is complete at 578 °C associated with a weight loss of 2.0 %. The sharp absorption peak of the IR spectrum for zincobotryogen at 3550 cm^{-1} could be attributed to the OH-stretching mode, the wide peak at 3420 cm^{-1} and the sharp peak at 1635 cm^{-1} to H_2O shown in Fig. 2 (Yang and Fu 1988a).

A Mössbauer spectrum had been measured by Yang and Fu (1988a) to determine the Fe valence state, revealing that there are two quadrupole doublets. The refined hyperfine parameters are IS (isomer shift) = 0.390 mm/s, QS (quadrupole splitting) = 1.131 mm/s for inner peaks; IS = 0.374 mm/s, QS = 1.629 mm/s for outer peaks. It indicates that iron atoms in this mineral belong to Fe^{3+}on two independent atomic sites. The ratio of areas of inner peaks to outer peaks is 36.3 : 63.7.

Table 4 Atomic coordinates and isotropic atomic displacement parameters (in Å^2) with estimated standard deviations (e.s.d.'s) in parentheses for zincobotryogen

Atom	*x*	*y*	*z*	U_{eq}
Fe(1)	0	0	0	0.01180(13)
Fe(2)	0	0	0.5	0.01451(14)
M[a]	0.40859(4)	0.18173(2)	0.34904(5)	0.01873(13)
S(1)	0.09275(7)	0.13894(4)	0.27867(9)	0.01330(15)
S(2)	0.70889(7)	0.06827(4)	0.88554(10)	0.01473(16)
O(1)	0.00992(19)	0.10571(11)	0.1082(3)	0.0155(4)
O(2)	0.21619(19)	0.16132(12)	0.2300(3)	0.0212(5)
O(3)	0.1173(2)	0.08029(12)	0.4307(3)	0.0187(4)
O(4)	0.0253(2)	0.20244(12)	0.3439(3)	0.0244(5)
O(5)	0.7426(2)	0.11666(12)	0.7336(3)	0.0240(5)
O(6)	0.80630(19)	0.00762(11)	0.9301(3)	0.0182(4)
O(7)	0.7064(2)	0.11350(13)	0.0576(3)	0.0255(5)
O(8)	0.5830(2)	0.03309(12)	0.8212(3)	0.0238(5)
O_H	0.0216(2)	0.04272(11)	0.7533(3)	0.0160(4)
H	0.071(3)	0.0749(18)	0.765(5)	0.024
O_W(1)	0.4498(2)	0.11727(14)	0.1258(4)	0.0270(5)
H(1A)	0.525(3)	0.119(2)	0.111(6)	0.04
H(1B)	0.437(4)	0.0717(19)	0.138(6)	0.04
O_W(2)	0.5987(2)	0.20426(15)	0.4561(4)	0.0316(6)
H(2A)	0.631(4)	0.244(2)	0.433(6)	0.047
H(2B)	0.638(4)	0.184(2)	0.554(5)	0.047
O_W(3)	0.3372(2)	0.24546(13)	0.5582(3)	0.0253(5)
H(3A)	0.395(3)	0.264(2)	0.640(5)	0.038
H(3B)	0.289(4)	0.278(2)	0.541(6)	0.038
O_W(4)	0.8331(2)	0.06166(14)	0.4193(3)	0.0262(5)
H(4A)	0.799(4)	0.079(2)	0.499(5)	0.039
H(4B)	0.796(4)	0.077(2)	0.317(5)	0.039
O_W(5)	0.4132(2)	0.27464(13)	0.1733(4)	0.0287(5)
H(5A)	0.451(4)	0.280(2)	0.088(5)	0.043
H(5B)	0.392(4)	0.315(2)	0.210(6)	0.043
O_W(6)	0.2050(3)	0.16113(16)	0.8252(4)	0.0333(6)
H(6A)	0.259(4)	0.145(2)	0.906(6)	0.05
H(6B)	0.249(4)	0.178(2)	0.750(6)	0.05
O_W(7)	0.4046(3)	0.08851(15)	0.5275(4)	0.0356(6)
H(7A)	0.460(4)	0.070(2)	0.617(6)	0.053
H(7B)	0.339(4)	0.067(2)	0.521(7)	0.053

[a] Occupancy: *M* = 0.836(3)Zn + 0.164(3)Mg

X-ray crystallography and crystal-structure refinement

Generalities

The X-ray powder diffraction data on zincobotryogen were obtained using a Bruker Smart APEX instrument with a CCD detector, monochromatized Mo$K\alpha$ (0.7107 Å) radiation at 45 kV and 35 mA, and using the GADDS program (Häming 2000). Observed d spacings are given in Table 2. Monoclinic unit cell parameters refined from the powder data are given as: $a = 10.49(1)$ Å, $b = 17.81(1)$ Å, $c = 7.187(9)$ Å, $\beta = 100.8(2)°$, $V = 1318(2)$ Å^3. The strongest lines in the powder X-ray diffraction pattern d(I)(hkl) are: 8.92 (100)(110), 6.32 (77)(−101), 5.56 (23)(021), 4.08 (22)(−221), 3.21 (31)(231), 3.03 (34)(032), and 2.77 (22)(042).

A single anhedral crystal was examined under a polarizing microscope with no indication of twinning. Single-crystal X-ray data for zincobotryogen were collected using monochromatic Mo$K\alpha$-radiation on a Rigaku RA-Micro7HF diffractometer with a Saturn 724+ CCD detector. A total of 1000 frames were recorded by a combination of several ω and φ rotation sets with a 0.5° scan width.

Data reduction, including intensity integration, correction for Lorentz and polarization effects, and absorption correction, was done using the software CrystalClear (Rigaku). Subsequent analysis of the intensity data by XPREP (Sheldrick 2003) indicated the centrosymmetric distribution of the normalized structure factors, allowing assignment of the unique space group $P12_1/n1$, with $a = 10.504(2)$, $b = 17.801(4)$, $c = 7.1263(14)$ Å, and $\beta = 100.08(3)°$, $V = 1311.9(5)$ Å^3, $Z = 4$. The crystal structure, based on the model of Süsse (1967, 1968) was refined using SHELX-97 (Sheldrick 1997). The refinement procedure was conducted by full-matrix least-squares techniques on F^2.

As the Mn and Fe^{2+} contents are low, only the Zn:Mg ratio at the octahedral M site was refined, assuming full site occupancy; the respective formula is $(Zn_{0.84}Mg_{0.16})Fe^{3+}(SO_4)_2(OH)\cdot 7(H_2O)$. The approximate positions of the H atoms of the H_2O and (OH) groups could be localized in difference-Fourier maps and were included in the final refinement, with isotropic atomic displacement parameters. Anisotropic displacement parameters were used for all other atoms. The crystal data, data-collection information and refinement details for zincobotryogen are listed in Table 3. The atomic coordinates, displacement parameters and site occupancy factors are shown in Tables 4 and 5. The relevant bond lengths and angles are shown in Table 6.

Table 5 Anisotropic displacement parameters (in Å^2) with estimated standard deviations (e.s.d.'s) in parentheses for zincobotryogen

Atom	U_{11}	U_{22}	U_{33}	U_{23}	U_{13}	U_{12}
Fe(1)	0.0132(3)	0.0138(3)	0.0084(3)	0.0001(2)	0.0017(2)	0.0003(2)
Fe(2)	0.0168(3)	0.0173(3)	0.0095(3)	0.0010(2)	0.0025(2)	0.0000(2)
M	0.0179(2)	0.0202(2)	0.0175(2)	0.00000(15)	0.00165(15)	−0.00026(16)
S(1)	0.0149(3)	0.0147(3)	0.0102(3)	−0.0008(2)	0.0020(3)	−0.0017(3)
S(2)	0.0131(3)	0.0159(3)	0.0149(3)	0.0007(3)	0.0016(3)	0.0012(3)
O(1)	0.0164(10)	0.0161(10)	0.0131(9)	−0.0015(8)	0.0000(8)	−0.0004(8)
O(2)	0.0153(10)	0.0297(12)	0.0176(10)	0.0036(9)	0.0006(8)	−0.0090(9)
O(3)	0.0211(11)	0.0216(11)	0.0127(10)	0.0041(8)	0.0014(8)	−0.0043(9)
O(4)	0.0316(13)	0.0200(11)	0.0221(11)	−0.0054(9)	0.0058(10)	0.0062(9)
O(5)	0.0230(11)	0.0253(12)	0.0246(11)	0.0092(9)	0.0067(9)	0.0027(9)
O(6)	0.0136(10)	0.0182(10)	0.0221(11)	0.0022(8)	0.0011(8)	0.0022(8)
O(7)	0.0254(12)	0.0295(12)	0.0227(11)	−0.0069(9)	0.0071(9)	0.0050(10)
O(8)	0.0126(10)	0.0242(11)	0.0318(12)	0.0030(10)	−0.0043(9)	−0.0024(9)
O_H	0.0196(11)	0.0179(11)	0.0107(9)	−0.0001(8)	0.0032(8)	−0.0046(8)
$O_W(1)$	0.0250(12)	0.0232(12)	0.0360(13)	−0.0066(10)	0.0144(11)	−0.0016(10)
$O_W(2)$	0.0256(13)	0.0305(14)	0.0351(14)	0.0070(11)	−0.0044(11)	−0.0033(10)
$O_W(3)$	0.0228(13)	0.0237(12)	0.0289(13)	−0.0069(10)	0.0028(10)	−0.0017(9)
$O_W(4)$	0.0277(13)	0.0354(14)	0.0157(11)	0.0039(10)	0.0040(10)	0.0142(10)
$O_W(5)$	0.0356(14)	0.0226(12)	0.0317(13)	0.0054(10)	0.0161(11)	0.0068(10)
$O_W(6)$	0.0316(14)	0.0462(16)	0.0216(13)	0.0040(11)	0.0033(11)	−0.0076(12)
$O_W(7)$	0.0288(14)	0.0331(15)	0.0394(15)	0.0156(11)	−0.0089(12)	−0.0022(11)

Table 6 Relevant bond lengths (Å) and angles (°) in zincobotryogen

$Fe(1)O_6$		$Fe(2)O_6$	
$Fe(1)–O_H$#1	1.9648(19)	$Fe(2)–O_H$#1	1.9349(19)
$–O_H$#2	1.9648(19)	$–O_H$	1.9350(19)
–O(6)#3	2.013(2)	–O(3)	2.005(2)
–O(6)#4	2.013(2)	–O(3)#1	2.005(2)
–O(1)	2.0294(19)	$–O_W$(4)#3	2.063(2)
–O(1)#5	2.0294(19)	$–O_W$(4)#6	2.063(2)
Mean	2.002	Mean	2.001
MO_6			
$M–O_W$(2)	2.049(3)	O_W(1)-M-O(2)	84.76(10)
$–O_W$(1)	2.068(2)	O(2)-M-O_W(5)	90.94(10)
–O(2)	2.080(2)	O_W(2)-M-O_W(5)	86.84(11)
$–O_W$(5)	2.082(2)	O_W(2)-M-O_W(1)	94.22(11)
$–O_W$(7)	2.096(3)	O_W(1)-M-O_W(5)	87.02(10)
$–O_W$(3)	2.112(2)	O_W(1)-M-O_W(7)	93.25(11)
Mean	2.081	O_W(7)-M-O_W(3)	87.12(11)
$S(1)O_4$		$S(2)O_4$	
S(1)–O(4)	1.453(2)	S(2)–O(8)	1.462(2)
–O(2)	1.455(2)	–O(7)	1.471(2)
–O(1)	1.487(2)	–O(5)	1.475(2)
–O(3)	1.494(2)	–O(6)	1.483(2)
Mean	1.472	Mean	1.473
H_2O			
H(1A)-O_W(1)-H(1B)	104(4)	H(5A)-O_W(5)-H(5B)	110(4)
H(2A)-O_W(2)-H(2B)	113(4)	H(6A)-O_W(6)-H(6B)	102(4)
H(3A)-O_W(3)-H(3B)	101(4)	H(7A)-O_W(7)-H(7B)	109(4)
H(4A)-O_W(4)-H(4B)	108(4)		

Symmetry code for equivalent positions: #1 = −x, −y, −z + 1; #2 = x, y, z-1; #3 = −x + 1, −y, −z + 1; #4 = x-1, y, z-1; #5 = −x, −y, −z; #6 = x-1, y, z

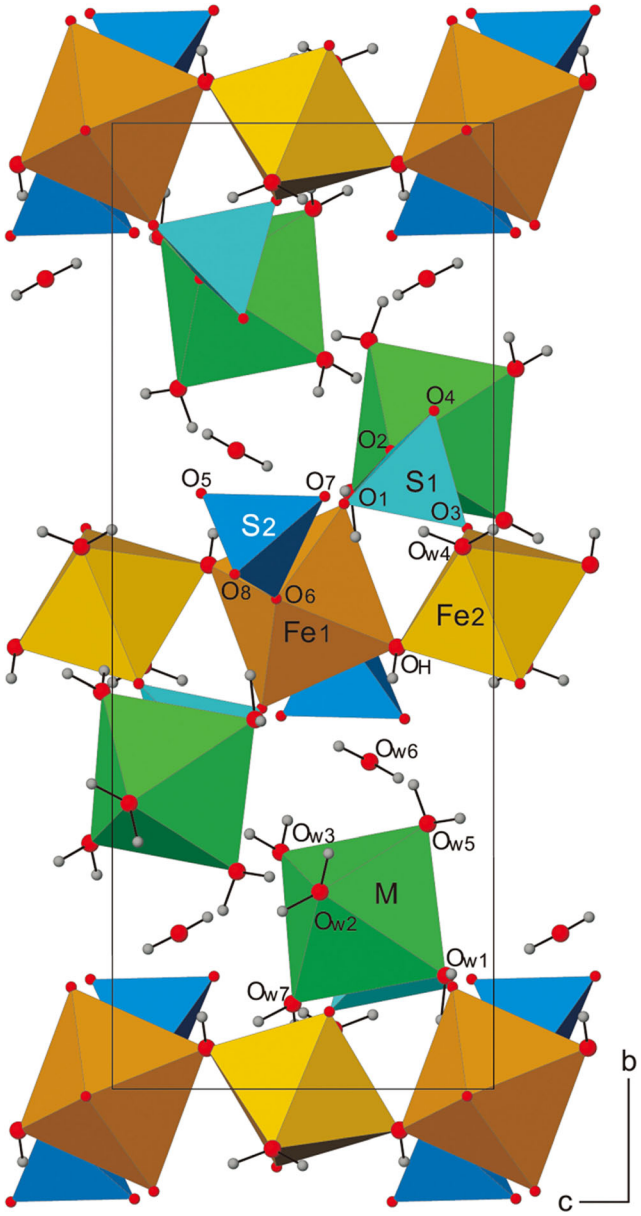

Fig. 3 The open-branched octahedral-tetrahedral chain in zincobotryogen viewed down the *a*-direction. $[Fe^{3+}(SO_4)_2(OH)(H_2O)]^{2-}$ chains with open-branched MO_6-polyhedra run parallel to the *c*-axis and are linked by hydrogen-bonds. All crystal structure drawings were done with ATOMS (Dowty 2013)

Structure description

The crystal structure of zincobotryogen corresponds to the model reported by Süsse (1967, 1968), Yang and Fu (1988a) and Majzlan et al. (2016). The structure of zincobotryogen is shown in a projection along the *b*-axis in Fig. 3. The atomic arrangement is characterized by chains of corner sharing $[Fe(1)O_4(OH)_2]$ and $[Fe(2)O_2(OH)_2(H_2O)_2]$ octahedra running parallel to the *c*-axis. Both atoms of ferric iron have site symmetry $\bar{1}$, Fe(1) is coordinated to four oxygen atoms of sulfate groups and to two of hydroxyl groups, Fe(2) to two oxygen atoms of sulfate groups, two of hydroxyl groups and two of H_2O molecules. Two independent sulfate tetrahedra, $S(1)O_4$ and $S(2)O_4$, attached via corners on alternate sides of the chain, provide further intra-chain linkages to constitute a structural building unit with composition $[Fe^{3+}(SO_4)_2(OH)(H_2O)]^{2-}$ and ~7 Å repeat distance, similar to that in sideronatrite-2 *M* (Yang et al. 2015). But, the chain in zincobotryogen links to a $[MO(H_2O)_5]$ octahedron through one of its vertices and the $[S(1)O_4]$ tetrahedron with an unshared H_2O molecule, and forms a larger chain building a module with composition $[M^{2+}Fe^{3+}(SO_4)_2(OH)(H_2O)_6(H_2O)]$. The packing of the chain modules in the structure is shown in Fig. 4; inter-chain module linkage involves only hydrogen bonding.

Both $[Fe(1)O_4(OH)_2]$ and $[Fe(2)O_2(OH)_2(H_2O)_2]$ octahedra are nearly regular. The average Fe–O distances, 2.002 and 2.001 Å, are close to those found in the structure of botryogen (2.002 and 1.998 Å, Majzlan et al. 2016), in sideronatrite-*2 M* (2.006 Å, Yang et al. 2015), in the orthorhombic polytype (1.999 Å, Scordari and Ventruti 2009), in the structure of metasideronatrite (2.008 Å, Ventruti et al. 2010), in chaidamuite (2.008 and 2.011 Å, Li and Wang 1990), or in $Fe^{3+}{}_2Fe^{2+}(SO_4)_4{\cdot}2(H_2O)$ (1.984 Å for ferric iron, Wildner and Giester 1991). The distances of $Fe(2)–O_H$ are shorter than those to O(1), O(6), O(3) and O_w(4) as similarly observed in the sideronatrite polytypes (Yang et al. 2015). The distances of

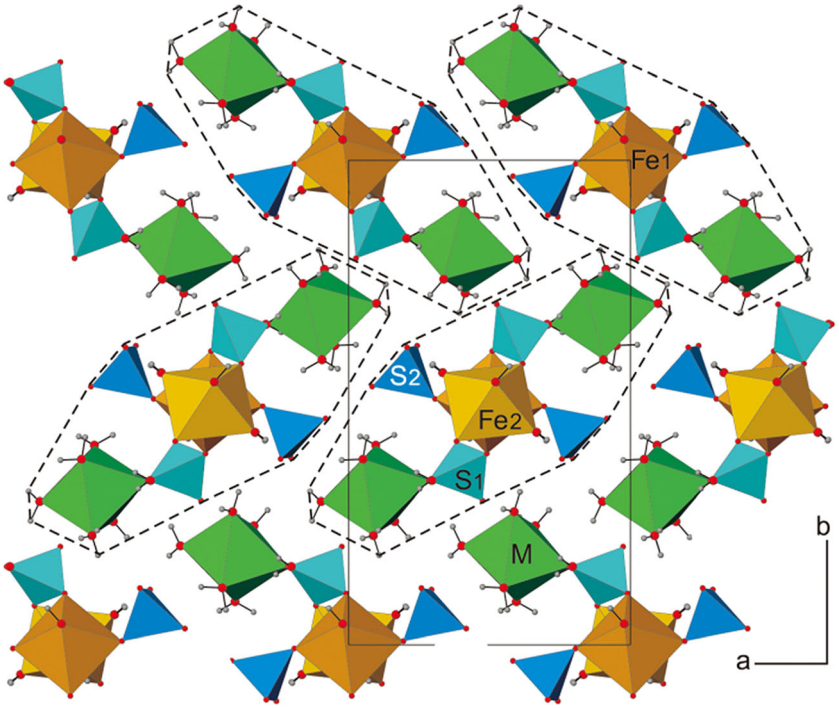

Fig. 4 Packing of chains in the zincobotryogen structure viewed down the *c*-direction. The chain modules are shown in broken lines

Fe(2)–O_W from iron to H_2O molecules are longer [2.063(2) Å].

The average S–O distances, 1.472 and 1.473 Å, fall in the range 1.47–1.48 Å reported for most hydrated sulfates (Palmer et al. 1972; Hawthorne et al. 2000). In the structure of botryogen, the average S–O distances are 1.471 and 1.470 Å (Majzlan et al. 2016).

The (MO_6) octahedron is nearly regular. The average M–O distance, 2.081 Å, can be compared with those found in the structure of botryogen (2.083 Å, Majzlan et al. 2016) and in chaidamuite, $ZnFe^{3+}(SO_4)_2(OH) \cdot 4H_2O$, [2.081 Å, (originally mistyped as 2.008 Å) for $Zn(1)O_6$, 2.114 Å for $Zn(2)O_6$, Li and Wang 1990].

System of hydrogen bonds

All hydrogen atoms have been approximately located in good agreement with the model proposed by Majzlan et al. (2016). Bond-valence theory allows estimating the reliability of a structure model. The bond-valence sums including contributions of hydrogen bonds, calculated from the O···O distances as suggested by Ferraris and Ivaldi (1988) (Tables 7 and 8), show satisfactory agreement with the valence-sum rule (Brown 2002). The valence sums of the bond strengths reaching each oxygen are quite satisfactory. The range of variation in S–O bond-valences is 1.421–1.588 *v.u.* (valence units), which is in accord with the bond-valence curve for S–O bond-valences (1.13–1.92 *v.u.*) given by Brown (1981) and Hawthorne et al. (2000).

The O_H atom shared between two consecutive Fe atoms is part of a hydroxyl group, whereas $O_w(1)$, $O_w(2)$, $O_w(3)$, $O_w(4)$,$O_w(5)$, $O_w(6)$, and $O_w(7)$ belong to H_2O molecules. The hydrogen bonding system is illustrated in Figs. 5 and 6. $O_w(6)$ is the only oxygen atom not linked to any cations, it

Table 7 Hydrogen-bond geometry (Å, °) for zincobotryogen

O–H···O	*d*(O–H)	*d*(H···O)	O–H···O	*d*(O···O)
O_H–H···$O_W(6)$	0.77(3)	2.074	174.09	2.841
$O_W(1)$–H(1A)···O(7)	0.81(3)	2.011	173.17	2.822
$O_W(1)$–H(1B)···O(8)#1	0.83(3)	1.905	176.33	2.733
$O_W(2)$–H(2A)···$O_W(6)$#2	0.82(3)	2.06	170.18	2.868
$O_W(2)$–H(2B)···O(5)	0.83(3)	1.949	163.91	2.753
$O_W(3)$–H(3A)···O(4)#3	0.84(3)	1.906	173.55	2.739
$O_W(3)$–H(3B)···O(7)#4	0.77(3)	2.128	160.69	2.862
$O_W(4)$–H(4A)···O(5)	0.79(3)	1.978	168.92	2.761
$O_W(4)$–H(4B)···O(7)	0.81(3)	2.027	178.13	2.84
$O_W(5)$–H(5A)···O(4)#5	0.79(3)	2.05	172.62	2.834
$O_W(5)$–H(5B)···O(5)#6	0.80(3)	2.023	145.65	2.722
$O_W(6)$–H(6A)···$O_W(1)$#7	0.79(3)	2.446	114.7	2.867
$O_W(6)$–H(6B)···$O_W(3)$	0.82(3)	2.144	167.26	2.954
$O_W(7)$–H(7A)···O(8)	0.85(3)	1.887	177.62	2.738
$O_W(7)$–H(7B)···O(3)	0.78(3)	2.316	142.93	2.978

Symmetry code for equivalent positions: #1 = −x + 1, −y, −z + 1;#2 = x + 1/2, −y + 1/2, z-1/2; #3 = x + 1/2, −y + 1/2, z + 1/2;#4 = x-1/2, −y + 1/2, z + 1/2;#5 = x + 1/2, −y + 1/2, z-1/2; #6 = x-1/2, −y + 1/2, z-1/2; #7 = x, y, z + 1

Table 8 Bond valences for zincobotryogen

	O(1)	O(2)	O(3)	O(4)	O(5)	O(6)	O(7)	O(8)	O_H	$O_W(1)$	$O_W(2)$	$O_W(3)$	$O_W(4)$	$O_W(5)$	$O_W(6)$	$O_W(7)$	Σ
Fe(1)	$0.482^{\times 2\rightarrow}$					$0.503^{\times 2\rightarrow}$			$0.573^{\times 2\rightarrow}$								3.12
Fe(2)			$0.514^{\times 2\rightarrow}$						$0.621^{\times 2\rightarrow}$				$0.440^{\times 2\rightarrow}$				3.15
M		0.360								0.372	0.391	0.330		0.358		0.345	2.16
S(1)	1.448	1.579	1.421	1.588													6.04
S(2)					1.464	1.496	1.512	1.549									6.02
H									0.830						0.170		1.00
H(1A)							0.176			0.824							1.00
H(1B)								0.211		0.789							1.00
H(2A)											0.838				0.162		1.00
H(2B)					0.202						0.798						1.00
H(3A)				0.208								0.792					1.00
H(3B)							0.163					0.837					1.00
H(4A)					0.199								0.801				1.00
H(4B)							0.170						0.830				1.00
H(5A)				0.172										0.828			1.00
H(5B)					0.216									0.784			1.00
H(6A)										0.162					0.838		1.00
H(6B)												0.140			0.860		1.00
H(7A)								0.209								0.791	1.00
H(7B)			0.135													0.865	1.00
	1.93	1.94	2.07	1.97	2.08	2.00	2.02	1.97	2.02	2.15	2.03	2.10	2.07	1.97	2.03	2.00	

The bond valences were calculated from the curves of Brese and O'Keeffe (1991); hydrogen bond strengths were calculated from the curves of Ferraris and Ivaldi (1988)

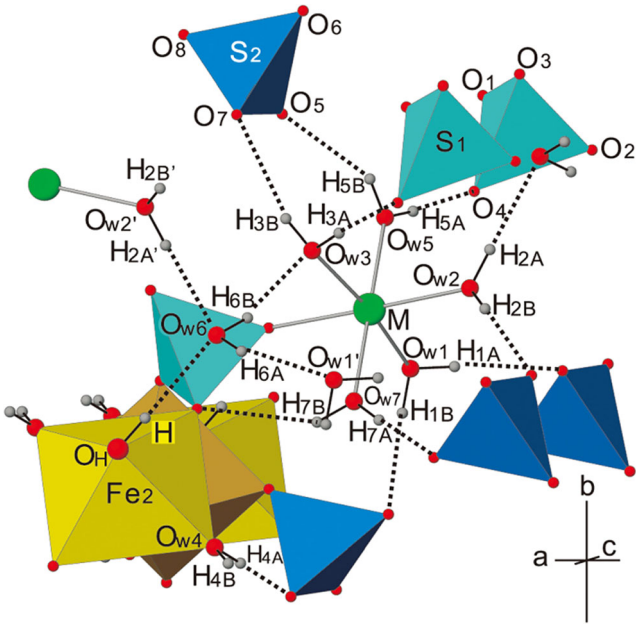

Fig. 5 The hydrogen-bond system in zincobotryogen seen along the *c*-direction

solely takes part in the hydrogen bonding system through four types of hydrogen bonds, $O_w(6)$-H(6A)···$O_w(1)$ and $O_w(6)$-H(6B)···$O_w(3)$, as well as $O_w(6)$···H, and $O_w(6)$···H(2A). $O_w(4)$ is the only not cross-linked oxygen atom between chain modules, and belongs to the hydrogen bonding system of the intra-chain module.

Adjacent chain modules in the structure are cross-linked through eight types of hydrogen bonds of five oxygen atoms of H_2O molecules, $O_w(1)$-H(1A)···O(7), $O_w(2)$-H(2A)···$O_w(6)$, $O_w(2)$-H(2B)···O(5), $O_w(3)$-H(3A)···O(4), $O_w(3)$-H(3B)···O(7), $O_w(5)$-H(5A)···O(4), $O_w(5)$-H(5B)···O(5), and $O_w(7)$-H(7A)···O(8) as shown in Figs. 5 and 6. The total strength of these eight types of hydrogen bonds from a chain building module with composition $[M^{2+}Fe^{3+}(SO_4)_2(OH)(H_2O)_6(H_2O)]$ to the adjacent ones is 1.508 *v.u.* (Table 8), which may represent the effective charge for zincobotryogen (Hawthorne and Schindler 2008). The ideal effective charge for this structural formula charge is 0 (the formal charge of the structural unit) -8×0.20 (the charge transferred by hydrogen bonding, assuming a hydrogen bond-valence of 0.20 *v.u.*) $=1.60^{-}$ (Hawthorne

Fig. 6 The hydrogen-bond system in zincobotryogen seen along the *a*-direction

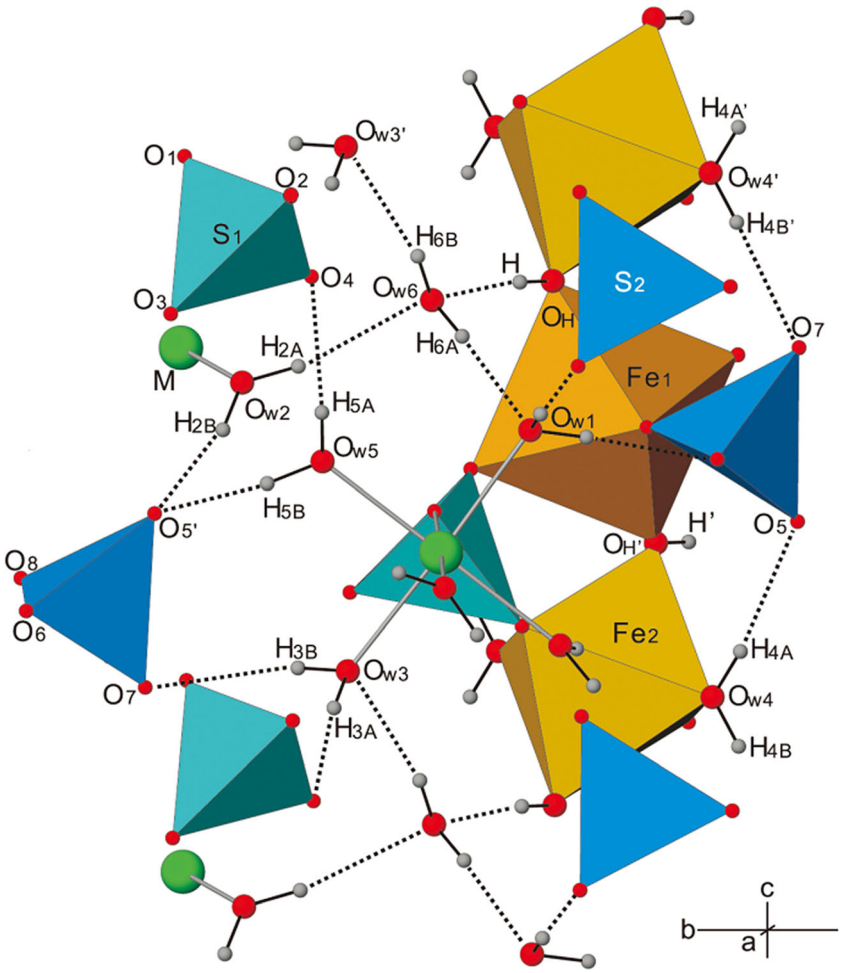

and Schindler 2008), which is approximately in agreement with the calculated value (1.508 *v.u.*).

Relationships to other minerals, and concluding remarks

Zincobotryogen belongs to the botryogen group (Strunz and Nickel: 07.DC.25; Dana: 31.09.06), which consists of two isotypic members: zincobotryogen is the Zn-end member, while botryogen, $MgFe^{3+}(SO_4)_2(OH)\cdot 7(H_2O)$, is the Mg-end member. In the structure of zincobotryogen, zinc, magnesium, manganese, and ferrous iron were assigned to the *M* site, ferric iron fully occupies the Fe sites. The calculated site scattering value (26.62 *epfu*) is in good agreement with the refined one (27.12 *epfu*), confirming the reliability of the model. "Botryogen" from the Rammelsberg mine, Germany, should be renamed as zincobotryogen, since zinc is the predominant element in the M site (Zemann 1961; Süsse 1967, 1968). The samples from Al-caparrosa locality, Antofagasta Province, Chile, and from Nuevo Cuyo, Argentina are botryogen, as magnesium is the predominant element in the *M* site (Frost et al. 2011; Majzlan et al. 2016).

Acknowledgments Open access funding provided by University of Vienna. The authors acknowledge the help of Hao Xiang and Liang Tongling with the single-crystal structure measurement. The project was supported by the National Natural Science Foundation of China (No. 41272063).

References

Brese NE, O'Keeffe M (1991) Bond-valence parameters for solids. Acta Cryst B47:192–197

Brown ID (1981) The bond-valence method: an empirical approach to chemical structure and bonding. In: O'Keeffe M, Navrotsky A (eds) Structure and bonding in crystals. Academic, New York, pp 1–30

Brown ID (2002) The chemical bond in inorganic chemistry: the bond valence model. Oxford Scientific Publication, UK

Dowty E (2013) Atoms V6.4.1 for atomic structure display. Shape Software, Kingsport

Ferraris G, Ivaldi G (1988) Bond valence vs. bond length in O···O hydrogenbonds. Acta Cryst B44:341–344

Frost RL, Palmer SJ, Cejka J, Sejkora J, Plasil J, Jebava I, Keeffe E (2011) A Raman spectroscopic study of $M^{2+}M^{3+}$sulfate minerals, römerite $Fe^{2+}Fe_2^{3+}(SO_4)_4\cdot 14H_2O$ and botryogen $Mg^{2+}Fe^{3+}(SO_4)_2(OH)\cdot 7H_2O$. J Raman Spectrosc 42:825–830

Häming L (2000) GADDS like experiments using SMART CCD detectors, quick guide, application scientist, single crystal diffraction. Bruker AXS GmbH, Karlsruhe

Hawthorne FC, Schindler M (2008) Understanding the weakly bonded constituents in oxysalt minerals. Z Kristallogr 223:41–68

Hawthorne FC, Krivovichev SV, Burns PC (2000) The crystal chemistry of sulfate minerals. In: Alpers CN, Jambor JL, Nordstrom BK (eds) Sulfate minerals: crystallography, geochemistry, and environmental significance. Rev Mineral Geochem l40:1–112

Lane MD, Bishop JL, Dyar MD, Hiroi TH, Mertzman SA, Bish DL, King PL, Rogers DR (2015) Mid-infrared emission spectroscopy and visible/near-infrared reflectance spectroscopy of Fe-sulfate minerals. Am Mineral 100:66–82

Li WM, Wang QG (1990) Determination and refinement of the crystal structure of chaidamuite. Sci China Chem 33:623–630

Majzlan J, Plasil J, Dachs E, Benisek A, Koch CB (2016) Crystal chemistry, Mössbauer spectroscopy, and thermodynamic properties of botryogen. J Mineral Geochem 193:147–159

Mandarino JA (1981) The Gladstone-Dale relationship: part IV the compatibility concept and its application. Can Mineral 19:441–450

Palmer KJ, Wong RY, Lee KS (1972) The crystal structure of ferric ammonium sulfate trihydrate, $FeNH_4(SO_4)_2\cdot 3H_2O$. Acta Cryst B28:236–241

Scordari F, Ventruti G (2009) Sideronatrite, $Na_2Fe(SO_4)_2(OH)\cdot 3H_2O$: crystal structure of the orthorhombic polytype and OD character analysis. Am Mineral 94:1679–1686

Sheldrick GM (1997) SHELXL-97, Program for the refinement of crystal structures. University of Göttingen, Germany

Sheldrick GM (2003) XPREP. Bruker-Nonius AXS, Madison

Süsse P (1967) Die Kristallstruktur des Botryogens. Naturwissenschaften 54:139

Süsse P (1968) Die Kristallstruktur des Botryogens. Acta Cryst B24:760–767

Tu KC, Li HL (1963) Studies on the characteristic features of the oxidation zone of the sulphide deposits in arid to extremely arid regions (with special reference to observations obtained from five sulphide deposits in the Northwestern China). Acta Geol Sin 43(4):361–377 (in Chinese with English abstract)

Tu KC, Li HL, Hsieh HD, Yin SS (1964a) Zincobotryogen and zincocopiapite–two new varieties of sulphate minerals. Acta Geol Sin 44:99–101 (in Chinese with English abstract)

Tu KC, Li HL, Hsieh HD, Yin SS (1964b) Zincobotryogen and zincocopiapite–two new varieties of sulphate minerals. Sci Geol Sin 5:313–330 (in Chinese)

Ventruti G, Stasi F, Scordari F (2010) Metasideronatrite: crystal structure and its relation with sideronatrite. Am Mineral 95:329–334

Wang LJ, Zhu XY, Wang JB, Deng JN (2008) A preliminary study on fluid inclusions and mineralization of Xitieshan sedimentary-exhalative (SEDEX) lead-zinc deposit. Acta Geol Sin-Engl 82:838–844

Wildner M, Giester G (1991) $Fe(II)Fe(III)_2(SO_4)_4\cdot 2H_2O$: a new Fe(II)-Fe(III) compound. Synthesis and crystal structure. Z Krist 196:269–277

Yang HX, Fu PQ (1988a) A further study of zincobotryogen. Acta Mineral Sin 8:119–224 (in Chinese with English abstract)

Yang HX, Fu PQ (1988b) Crystal structure of zincobotryogen. Acta Mineral Sin 8:1–12 (in Chinese with English abstract)

Yang ZM, Giester G, Ding KS, Li H (2015) Crystal structure of sideronatrite-2*M*, $Na_2Fe(SO_4)_2(OH)(H_2O)_3$, a new polytype from Xitieshan lead-zinc deposit, Qinghai Province, China. Eur J Mineral 27:427–432

Zemann J (1961) Über den Botryogen vom Rammelsberg. Fortschr Mineral 39:84